A Journal of the Gesellschaft Deutscher Chemiker

Angewandte International Edition

GDCh

Chemie

www.angewandte.org

Accepted Article

Title: A sugar sorting pathway directed bioorthogonal conjugation enables continual tracking of stressed organelles

Authors: Shoufa Han, Zhongwei Xue, Enkang Zhang, Jian Liu, and Jiahuai Han

To be cited as: *Angew. Chem. Int. Ed.* 10.1002/anie.201802972
Angew. Chem. 10.1002/ange.201802972

Link to VoR: http://dx.doi.org/10.1002/anie.201802972
http://dx.doi.org/10.1002/ange.201802972

WILEY-VCH

10.1002/anie.201802972

WILEY-VCH

A sugar sorting pathway directed bioorthogonal conjugation enables continual tracking of stressed organelles

Zhongwei Xue,[a, ‡] Enkang Zhang,[a, ‡] Jian Liu,[a] Jiahuai Han,[b] and Shoufa Han[a,*]

Abstract: Selective and continuous tracking of dynamic organelles are crucial for modern biology. We herein reported a ship-in-bottle strategy to tag lysosomes using strain-promoted azide-alkyne cycloaddition to couple a pH sensor (RC) with mannose-6-carboxylate (M6C) actively transported into lysosomes via cell sorting. Relative to classical acidotropic sensors prone to dissipate from lysosomes, *in situ* formed M6C-RC is stably trapped in lysosomes without resort to lysosomal acidity, exhibiting "always-on" blue fluorescence to pinpoint lysosomes and red-to-blue fluorescence ratios indicative of lysosomal pH. These advantages enable tracking of stressed lysosomes and discern of lysosomal pH changes in necrosis over apoptosis. The cell sorting-mediated bioorthogonal tagging strategy offers a new route to track stressed organelles with disrupted physiological organelle-probe affinity.

Fluorescence imaging aided with advancing labeling technologies provides unprecedented opportunities for spatiotemporal visualization of diverse biological processes at realms scaling from biomolecules to organelles and to whole organisms.[1] Cell fates are largely shaped by combined activity of distinct subcellular organelles, which are often targeted with synthetic probes driven by organelle parameters such as mitochondrial potentials and lysosomal acidity.[2] Albeit widely used, these probes are prone to dissipate upon organelle stress such as loss of lysosomal acidity. Lysosomes are acidic organelles essential to myriad cellular events including immunity, cell homeostasis, and cell death.[3] Abnormal lysosomes are manifested in numerous pathological conditions.[4] For example, lysosomal pH is markedly elevated in lysosomal storage diseases,[5] while altered lysosome positioning occurs in cancer metastasis.[6] As such, approaches capable of continual tracking of stressed lysosomes are of use to decipher the roles of lysosomes in biology and diseases.

Herein we report a sugar sorting pathway directed intraorganelle bioorthogonal conjugation (SPIBC) to tag lysosomes whereby dibenzocyclooctyne (DBCO) appended mannose-6-caboxylate (^{DBCO}M6C) is actively transported into lysosomes through endogenous mannose-6-phosphate (M6P) sorting pathway, and then undergoes strain-promoted azide-alkyne cycloaddtion with diffusible an azide-bearing rhodamine-lactam/coumarin diad (^{Az}RC) to give M6C-RC in lysosomes (Figure 1). *In situ* formed M6C-RC is maintained in lysosomes independent of lysosomal acidity and exhibits pH relevant ratiometric fluorescence, which enable tracking of lysosome alterations in exocytosis and cell death signaling events.

Lysosomes are routinely imaged with sensors that accumulate in lysosomes driven by protonation.[2] However these acidotropic sensors are prone to dissipate from lysosomes upon pH elevation. For instance, a rhodamine-lactam based pH sensor suffers from significant signal loss from stressed lysosomes in apoptosis.[7] In view of this limitation, we sought to trap diffusible optical sensors through bioorthogonal conjugation with an entity that could be maintained in lysosomes independent of lysosomal acidity. Ubiquitous in mammalian cells, M6P receptors mainly address newly biosynthesized hydrolases with M6P-terminating glycans to lysosomes.[8] M6P is degradable by phosphatases. As the structural analog of M6P, M6C possesses a lateral carboxylate bridged by a methylene linker and is immune to phosphatase hydrolysis,[9] To hijack M6P sorting pathway, M6C was used as the lysosome-localizing entity to conjugate pH-reporting ^{Az}RC in lysosomes (Figure 1).[10]

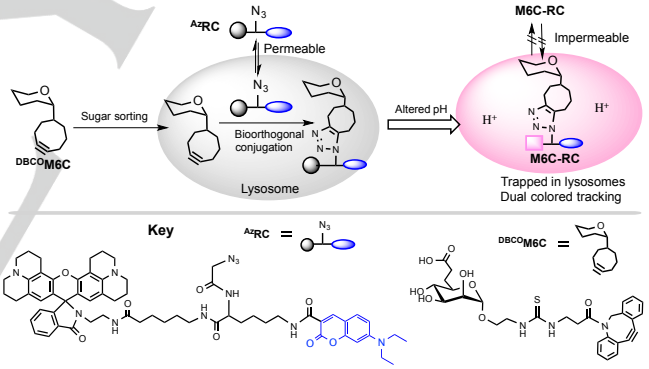

Figure 1. Schematic for lysosome imaging by a sugar sorting pathway directed intralysosomal bioorthogonal conjugation (SPIBC). Delivered into lysosomes by M6P sorting, ^{DBCO}M6C reacts with ^{Az}RC via azide-alkyne cycloaddition to give M6C-RC, which is stably trapped in lysosomes and gives pH-relevant ratiometric fluorescence. The key shows chemical structures of ^{BCO}M6C and ^{Az}RC.

We hence prepared ^{DBCO}M6C and ^{Az}RC, which readily combined in vitro to give M6C-RC as a mixture of two regioisomers as evidenced by HPLC and mass spectrometry analysis (Figure S1-S2, Supporting Information). pH titration shows that M6C-RC and RC both display "always-on" blue coumarin fluorescence (CM) moderately declining as pH decreases, and acidity mediated "turn-on" rhodamine-X fluorescence (ROX) which intensified as pH decreased (pH 6.5−4.5) (Figure 2, Figure S3, Supporting Information), owing to proton mediated fluorogenic isomerization of rhodamine-lactam (Figure 2A).[7, 11] Ratiometric imaging affords enhanced accuracy relative to single intensity fluorescence imaging.[12] The sensitive blue-to-red fluorescence ratios of M6C-RC in pH 6.0−4.5 are

[a] Z. Xue, E. Zhang, Dr. J. Lu, Prof. S. Han
State Key Laboratory for Physical Chemistry of Solid Surfaces, Department of Chemical Biology, College of Chemistry and Chemical Engineering, the Key Laboratory for Chemical Biology of Fujian Province, The MOE Key Laboratory of Spectrochemical Analysis & Instrumentation, and Innovation Center for Cell Signaling Network, Xiamen University;
E-mail: shoufa@xmu.edu.cn
‡ Both authors contributed equally to this work.
[b] Prof. J. Han
State key Laboratory of Cellular Stress Biology, Innovation Center for Cell Signaling Network, School of Life Sciences, Xiamen University, Xiamen, 361005, China

Supporting information for this article is given via a link at the end of the document.

beneficial to monitor subtle changes of lysosomal acidity (Figure 2D).

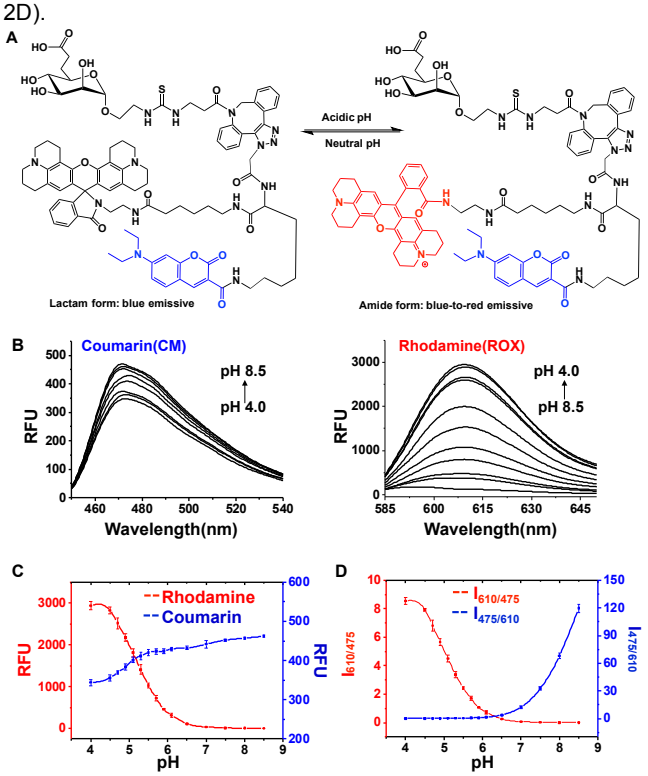

Figure 2. pH mediated ratiometric fluorescence of M6C-RC. (**A**) Proton triggered isomerization of M6C-RC gives "turn-on" ROX fluorescence. (**B**) CM and ROX fluorescence of M6C-RC (5 μM) at pH 4.5−8.5 (λ_{ex}: 435 nm for CM, 590 nm for ROX). (**C**) pH titration curves of M6C-RC; fluorescence emission of ROX (λ_{em}:605 nm) and CM (λ_{em}:475 nm) were plotted over pH. (**D** pH dependent fluorescence ratios of ROX (I_{610}) to CM (I_{475}).

To ascertain SPIBC-mediated targeting of lysosomes, HeLa cells expressing GFP-Lamp2 (green fluorescent protein-fused lysosome associated membrane protein 2) were cultivated with ^{DBCO}M6C/^{Az}RC. Confocal microscopy analysis revealed bright and punctate ROX and CM signals, which eclipsed GFP-Lamp2 in cells stained with ^{DBCO}M6C/^{Az}RC (Figure 3A). As Lamp2-GFP is a protein marker specific for lysosomes, colocalization of CM/ROX signals with GFP-Lamp2 proves stringent selectivity of SPIBC for lysosome imaging. Relative to in vitro synthesized M6C-RC, staining with ^{DBCO}M6C/^{Az}RC exhibits much brighter lysosomal fluorescence and is kinetically favored (Figure S4, Supporting Information), validating that ^{DBCO}M6C is preferentially delivered into lysosomes over M6C-RC by cells. In addition, lysosomes were effectively illuminated with ^{DBCO}M6C/^{Az}RC in a variety of cell lines including A549, L929, and MCF-7 cells (Figure S5, Supporting Information), proving the applicability of SPIBC for effective lysosome imaging in diverse cell lines.

To assess lysosomal retention of *in situ* formed M6C-RC, GFP-Lamp2^{+} HeLa cells was treated with ^{DBCO}M6C/^{Az}RC in the presence of Baflomycin A1, which is a potent inhibitor of V-ATPase and neutralizes lysosomes. The loss of ROX signals observed in Baflomycin A1-treated cells is in line with acidity mediated ROX fluorescence (Figure 4). By contrast, discrete CM signals remained intensive and colocalized with GFP-Lamp2 in cells (Figure 4, Figure S6, Supporting Information), proving retention of M6C-RC in lysosomes is independent of lysosomal acidity. Relative to hydrophilic ^{Az}RC, in situ generated M6C-RC is rather hydrophilic, which could hinder diffusion across the lysosomal membrane and thus contribute to acidity-independent retention of M6C-RC in lysosomes (Figure 1).

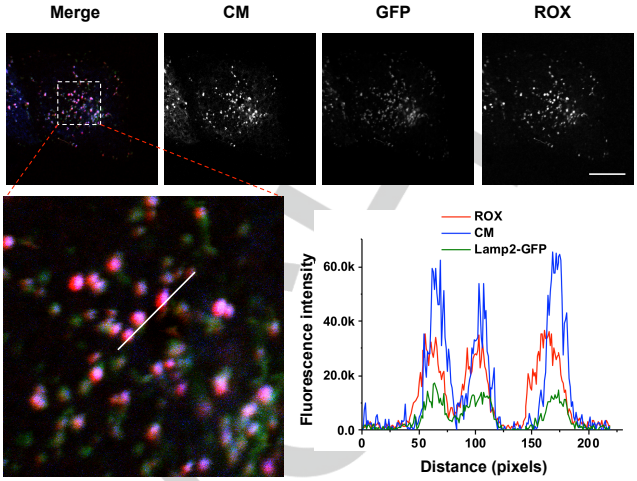

Figure 3. SPIBC-mediated selective imaging of lysosomes. GFP-Lamp2^{+} HeLa cells stained with ^{DBCO}M6C/^{Az}RC were probed by confocal microscopy. Plots of fluorescence of CM, ROX, and GFP were measured along the line shown in zoomed images, which reveals colocalization of CM/ROX signals with Lamp2-GFP. Scale bar, 10 μm.

We next probed the structural factors required for SPIBC. ^{Az}RC is prone to protonation of the spirolactam to give the amide form (Figure S3, Supporting Information), which enable acidity-dependent lysosomal staining. As expected HeLa cells treated with ^{Az}RC alone displayed loss of lysosome-associated fluorescence upon Baflomycin A1 treatment (Figure 4), a phenomenon characteristic of acidotropic sensors owing to dissipation form neutralized lysosomes, highlighting the essential role of ^{DBCO}M6C in SPIBC. Relative to ^{DBCO}M6C, ^{amino}M6C is devoid of the DBCO moiety while DBCO-conjugated mannose (^{DBCO}M) lacks the lateral carboxylate group. Baflomycin A1 triggered loss of ^{Az}RC from lysosomes was also observed in cells co-stained with ^{amino}M6C or ^{DMCO}M (Figure 4), which validates the crucial roles of DBCO moiety and carboxylate group of ^{DBCO}M6C in SPIBC. Likewise, cells cultivated with ^{DBCO}M6C and azide-free RC display vanished ROX/CM fluorescence upon Baflomycin A1-mediated lysosomal neutralization (Figure S7, Supporting Information), validating the dependence of the azido moiety of ^{Az}RC for SPIBC mediated acidity independent imaging.

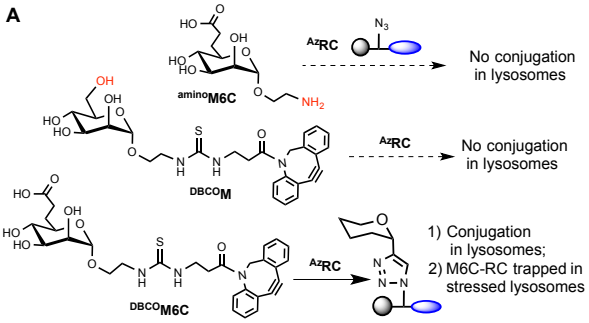

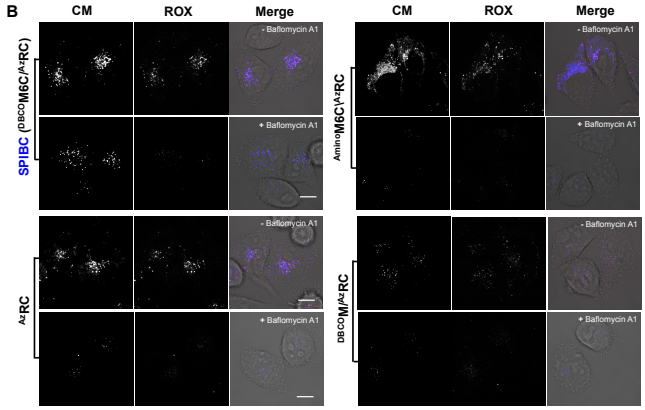

Figure 4. Acidity-independent lysosomal imaging by SPIBC. (**A**) Chemical structures of ^{amino}M6C and ^{DBCO}M as compared to ^{DBCO}M6C. (**B**) Confocal microscopic images of ^{Az}RC-treated HeLa cells that were respectively cultured with ^{DBCO}M6C, ^{Amino}M6C, ^{DBCO}M or no addition in the presence or absence of Baflomycin A1. Scale bar, 10 μm.

GFP-Lamp2^{+} HeLa cells were treated with chloroquine to introduce lysosomal membrane permeabilization.[13] SPIBC analysis revealed decreased colocalization of CM with GFP (Figure S8, Supporting Information), indicative of leakage of M6C-RC from permeabilized lysosomes, showing that membrane integrity is required for SPIBC-based imaging. These results establish that the azido group of ^{Az}RC, and M6C/DBCO domains of ^{DBCO}M6C are prerequisites for SPIBC. SPIBC was significantly inhibited at 4 °C relative to 37 °C (Figure S9, Supporting Information), supporting involvement of membrane trafficking in transport of ^{DBCO}M6C into lysosomes by membrane anchored M6P receptor. In addition, we observed dose-dependent inhibition on SPIBC by exogenous M6P (Figure S10, Supporting Information), the natural ligand of M6P receptor. The competition between M6P and ^{DBCO}M6C validates involvement of M6P sorting in SPIBC. Given the liability of acidotropic dyes to leak from neutralized lysosomes, the acidity independent SPIBC-based imaging offers unprecedented choices to track cellular events featuring lysosomal pH elevation.

Lysosomal exocytosis underlies a number of critical cellular functions such as plasma membrane repair, transmitter release, and immune degranulation.[14] Exocytosis is elusive to image owing to loss of acidotropic dyes from exocytosizing lysosomes. As such distinct approaches have been developed to image exocytosis.[15] Shown to stain lysosomes without resort to lysosomal acidity, SPIBC was evaluated for its efficacy to image exocytosis. RBL-2H3 cells loaded with ^{DBCO}M6C/^{Az}RC were stimulated with ionomycin, a calcium ionophore capable of stimulating lysosome exocytosis.[16] We observed lysosomes exhibited punctate CM signals and diminished ROX fluorescence in the vicinity of cell surface in Ionomycin^{+} cells (Figure S11, Supporting Information). The loss of ROX signals is consistent with previous observation on lysosomal pH elevation upon exocytosis,[17] and the bright CM fluorescence show retention of in situ conjugated M6C-RC in lysosomes during exocytosis. The capability of SPIBC to track exocytosing lysosomes proves its utility for spatiotemporal visualization of dynamic lysosomes with altered lysosomal pH and positioning in live cells.

Deregulated cell death is a common feature of several diseases such as cancers. Cell death occurs through a number of distinct routes,[18] whereby lysosomes participate in distinct cell death pathways.[3a, 19] Apoptosis is considered cell autonomous and non-inflammatory whereas necrosis often leads to inflammation.[20] We then applied SPIBC to image lysosomal responses in cell death using RIP3^{+} (receptor-interacting protein 3) HeLa cells treated with Smac and human Tumor Necrosis Factor-a (TNF) to trigger apoptosis, or with Smac/TNF/Z-VAD to trigger necroptosis, a programmed form of necrosis.[21] Time course analysis by bivariate dot-plots of forward scatter (FSC) versus side scatter (SSC) clearly revealed formation of two new cell populations (Figure 5a, d), owing to apoptosis and necrosis as confirmed by Western Blotting analysis and staining with Annexin-V/propidium iodide (Figure S12-13, Supporting Information). The dot-plots of ROX vs CM, indicative of lysosomal pH, show that apoptosed cells display attenuated ROX/CM ratios of similar magnitudes as apoptosing cells whereas necrosed cells feature substantially decreased ROX/CM ratios over necrosing cells (Figure 5b, e). In addition, confocal microscopy confirmed obviously declined ROX fluorescence and ROX/CM ratios in necrosed cells relative to necrosing cells (Figure 6). Apart from the common tendency to loose lysosomal acidity in both cell death modalities, these results show that lysosomal pH elevation is greater in necrosed cells than necrosing cells, but remained alike in apoptosed cells and apoptosing cells, demonstrating the utility of SPIBC to discern lysosome changes in closely related cell death subtypes.

Metabolic bioorthogonal labeling in biological systems enables visualization of various biomolecules including glycans, nucleic acids, and lipids.[22] In the context of these advances, we show the use of sugar sorting pathway mediated intralysosomal bioorthogonal conjugation for imaging of stressed lysosomes, which represents a further extension of bioorthogonal chemistry in bioimaging.

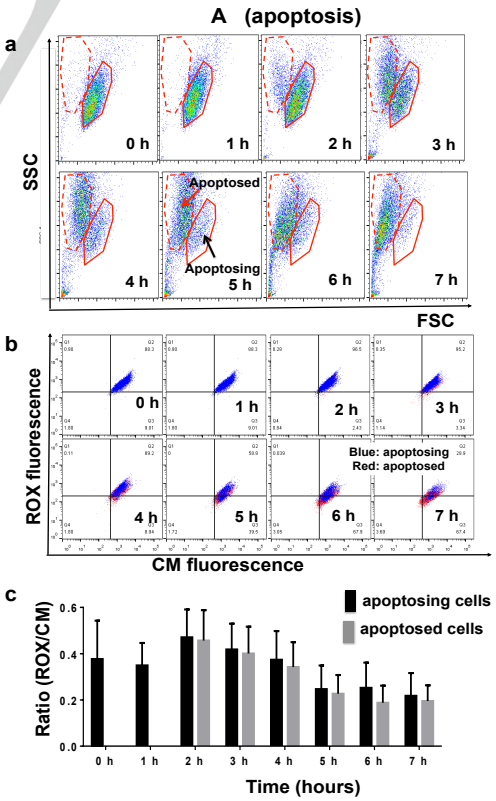

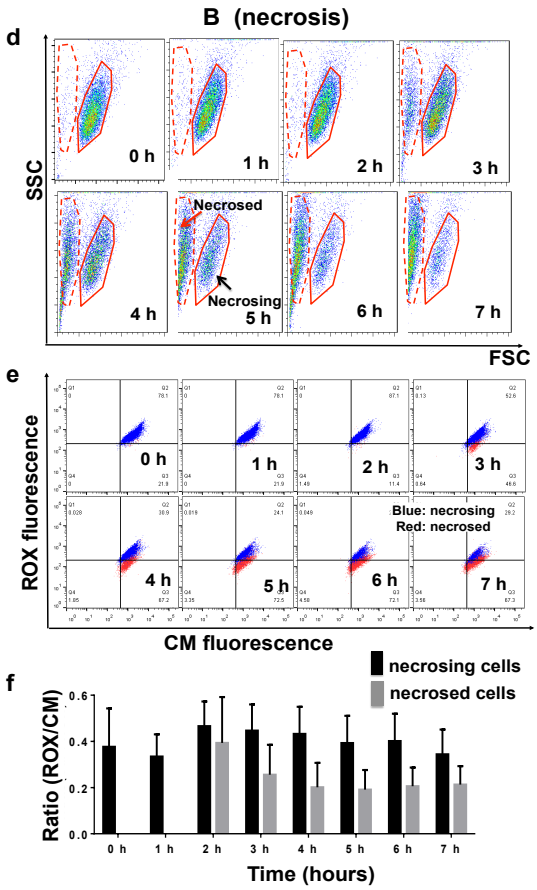

Figure 5. Distinct lysosomal pH alteration profiles in apoptosis and necroptosis revealed by SPIBC. RIP_3^+ HeLa cells prestained with ^{DBCO}M6C/^{Az}RC were cultivated with TNF/Smac (**A**) or TNF/Smac/Z-VAD (**B**) and then monitored over time by flow cytometry. Cell populations in CM vs ROX dot-plots (**b, e**) were gated identically as those in bivariate dot-plots of FSC vs SSC (**a, d**). Statistical results of ROX/CM ratios were measured by flow cytometry (**c** and **f**). Error bars represent standard deviation of 10000 cells.

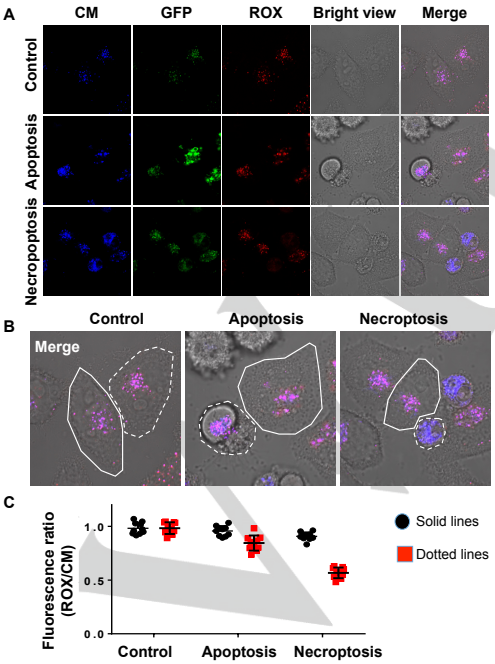

Figure 6. Discerning lysosomal pH changes in apoptosis over necroptosis with SPIBC. (**A**) RIP_3^+/Lamp2-GFP^+ HeLa cells loaded with ^{DBCO}M6C/^{Az}RC were further cultivated with TNF/Smac or TNF/Smac/Z-VAD before confocal microscopy analysis. (**B**) Apoptosed cells and necrosed cells were enclosed by dotted line in the zoomed images. Apoptosing cells and necrosing cells were indicated by solid lines. (**C**) Statistical results of ROX/CM ratios were measured by confocal microscopy. Error bars represent standard deviation of 10 representative cells. Scale bars, 10 μm.

In conclusion, we demonstrated a ship-in-bottle strategy to track stressed lysosomes using sugar sorting pathway directed bioorthogonal conjugation. Actively transported into lysosomes through cellular M6P sorting, ^{DBCO}M6C undergoes strain-promoted azide-alkyne cycloaddition with ^{Az}RC in lysosomes. In situ formed M6C-RC, stably maintained in lysosomes without resort to lysosomal acidity, enables spatiotemporal tracking of stressed lysosomes and discerning of lysosomal pH changes in necroptosis over apoptosis. Manifested in myriad diseases, stressed organelles are often challenging to track with classical organelle sensors owing to frequent loss of physiological organelle-probe affinity. Apart from visualizing stressed lysosomes, SPIBC holds potentials to be adapted to other specific organelles with the aid of cognate organelle-destined trafficking or sorting pathways, representing a new perspective from which to probe organelle stress in biology and diseases.

Supporting Information available on experimental procedures, confocal microscopy analysis of cell staining with M6C-RC, effects of temperature and M6P on SPIBC, PI/Annexin-V staining, western blotting and cell cytotoxicity assay.

Acknowledgements

This work was supported by grants from NSF China (21775130, 21572189, 21602185), and the Fundamental Research Funds for the Central Universities (20720160052, 20720150047), Xiamen University; Dr J. Han was supported by the National Basic Research Program of China (973 Program, 2015CB553800) and grants from NSF China (81788101, 31420103910, 31330047, 81630042).

Keywords: Stressed organelle • ratiometric fluorescence imaging • sugar sorting pathway• bioorthogonal reaction • cell death

[1] (a) F. Leblond, S. C. Davis, P. A. Valdes, B. W. Pogue, *J Photochem. Photobiol. B* **2010**, *98*, 77-94; (b) K. M. Dean, A. E. Palmer, *Nat. Chem. Biol.* **2014**, *10*, 512-523; (c) S. H. Shim, C. Xia, G. Zhong, H. P. Babcock, J. C. Vaughan, B. Huang, X. Wang, C. Xu, G. Q. Bi, X. Zhuang, *Proc. Natl. Acad. Sci. USA* **2012**, *109*, 13978-13983; (d) E. M. Sevick-Muraca, *Annu. Rev. Med.* **2012**, *63*, 217-231.

[2] C. de Duve, T. de Barsy, B. Poole, A. Trouet, P. Tulkens, F. Van Hoof, *Biochem. Pharmacol.* **1974**, *23*, 2495-2531.

[3] aG. Kroemer, M. Jaattela, *Nat. Rev. Cancer* **2005**, *5*, 886-897; bP. Saftig, J. Klumperman, *Nat. Rev. Mol. Cell Biol.* **2009**, *10*, 623-635.

[4] C. Settembre, A. Fraldi, D. L. Medina, A. Ballabio, *Nat. Rev. Mol. Cell Biol.* **2013**, *14*, 283-296.

[5] A. Kogot-Levin, M. Zeigler, A. Ornoy, G. Bach, *Pediatr. Res.* **2009**, *65*, 686-690.

[6] N. Fehrenbacher, M. Jaattela, *Cancer Res.* **2005**, *65*, 2993-2995.

[7] Z. Xue, H. Zhao, J. Liu, J. Han, S. Han, *ACS Sens.* **2017**, *2*, 436-442.

[8] (a) P. Ghosh, N. M. Dahms, S. Kornfeld, *Nat. Rev. Mol. Cell Biol.* **2003**, *4*, 202-212; (b) M. Gary-Bobo, P. Nirde, A. Jeanjean, A. Morere, M. Garcia, *Curr. Med. Chem.* **2007**, *14*, 2945-2953.

[9] (a) A. Jeanjean, M. Garcia, A. Leydet, J. L. Montero, A. Morere, *Bioorg. Med. Chem.* **2006**, *14*, 3575-3582; (b) O. Vaillant, K. El Cheikh, D. Warther, D. Brevet, M. Maynadier, E. Bouffard, F. Salgues, A. Jeanjean, P. Puche, C. Mazerolles, P. Maillard, O. Mongin, M. Blanchard-Desce, L. Raehm, X. Rebillard, J. O. Durand, M. Gary-Bobo, A. Morere, M. Garcia, *Angew. Chem. Int. Ed. Engl.* **2015**, *54*, 5952-5956.

[10] (a) N. J. Agard, J. A. Prescher, C. R. Bertozzi, *J. Am. Chem. Soc.* **2004**, *126*, 15046-15047; (b) J. C. Jewett, C. R. Bertozzi, *Chem. Soc. Rev.* **2010**, *39*, 1272-1279.

[11] (a) W. Zhang, B. Tang, X. Liu, Y. Liu, K. Xu, J. Ma, L. Tong, G. Yang, *Analyst* **2009**, *134*, 367-371; (b) T. Hasegawa, Y. Kondo, Y. Koizumi, T. Sugiyama, A. Takeda, S. Ito, F. Hamada, *Bioorg. Med. Chem.* **2009**, *17*, 6015-6019; (c) X. Wu, M. Yu, B. LIin, J. Han, S. Han, *Chem. Sci.* **2015**, *6*, 798-803; (d) M. Yu, X. Wu, B. Lin, J. Han, L. Yang, S. Han, *Anal. Chem.* **2015**, *87*, 6688-6695; (e) Z. Xue, H. Zhao, J. Liu, J. Han, S. Han, *Chem. Sci.* **2017**, *8*, 1915-1921.

[12] (a) Q. Wang, L. Zhou, L. Qiu, D. Lu, Y. Wu, X. B. Zhang, *Analyst* **2015**, *140*, 5563-5569; (b) X. Z. Zhang, T.; Shen, S.; Miao, J.; Zhao, B. , *J. Mater. Chem. B* **2015**, *3*, 3260−3266; (c) G. Li, D. Zhu, L. Xue, H. Jiang, *Org. Lett.* **2013**, *15*, 5020-5023; (d) B. Dong, X. Song, C. Wang, X. Kong, Y. Tang, W. Lin, *Anal. Chem.* **2016**, *88*, 4085−4091; (e) Z. Li, S. Wu, J. Han, L. Yang, S. Han, *Talanta* **2013**, *114*, 254-260; (f) G. J. Song, S. Y. Bai, J. Luo, X. Q. Cao, B. X. Zhao, *J. Fluoresc.* **2016**, *26*, 2079-2086.

[13] K. R. Schultz, A. L. Gilman, *Leuk. Lymphoma* **1997**, *24*, 201-210.

[14] E. D. Gundelfinger, M. M. Kessels, B. Qualmann, *Nat. Rev. Mol. Cell Biol.* **2003**, *4*, 127-139.

[15] (a) D. Asanuma, Y. Takaoka, S. Namiki, K. Takikawa, M. Kamiya, T. Nagano, Y. Urano, K. Hirose, *Angew. Chem. Int. Ed. Engl.* **2014**, *53*, 6085-6089; (b) D. Zenisek, J. A. Steyer, W. Almers, *Nature* **2000**, *406*, 849-854; (c) G. Miesenbock, D. A. De Angelis, J. E. Rothman, *Nature* **1998**, *394*, 192-195; (d) D. Liu, J. A. Martina, X. S. Wu, J. A. Hammer, 3rd, E. O. Long, *Immunol. Cell Biol.* **2011**, *89*, 728-738.

[16] A. Rodriguez, P. Webster, J. Ortego, N. W. Andrews, *J. Cell Biol.* **1997**, *137*, 93-104.

[17] H. Xu, D. Ren, *Annu. Rev. Physiol.* **2015**, *77*, 57-80.

[18] (a) G. Kroemer, L. Galluzzi, P. Vandenabeele, J. Abrams, E. S. Alnemri, E. H. Baehrecke, M. V. Blagosklonny, W. S. El-Deiry, P. Golstein, D. R. Green, M. Hengartner, R. A. Knight, S. Kumar, S. A. Lipton, W. Malorni, G. Nunez, M. E. Peter, J. Tschopp, J. Yuan, M. Piacentini, B. Zhivotovsky, G. Melino, *Cell Death Differ.* **2009**, *16*, 3-11; (b) S. J. Dixon, K. M. Lemberg, M. R. Lamprecht, R. Skouta, E. M. Zaitsev, C. E. Gleason, D. N. Patel, A. J. Bauer, A. M. Cantley, W. S. Yang, B. Morrison, B. R. Stockwell, *Cell* **2012**, *149*, 1060-1072; (c) M. Overholtzer, A. A. Mailleux, G. Mouneimne, G. Normand, S. J. Schnitt, R. W. King, E. S. Cibas, J. S. Brugge, *Cell* **2007**, *131*, 966-979.

[19] S. Aits, M. Jaattela, *J. Cell Sci.* **2013**, *126*, 1905-1912.

[20] T. Vanden Berghe, A. Linkermann, S. Jouan-Lanhouet, H. Walczak, P. Vandenabeele, *Nat. Rev. Mol. Cell Biol.* **2014**, *15*, 135-147.

[21] S. He, L. Wang, L. Miao, T. Wang, F. Du, L. Zhao, X. Wang, *Cell* **2009**, *137*, 1100-1111.

[22] (a) C. Y. Jao, M. Roth, R. Welti, A. Salic, *Proc. Natl. Acad. Sci. USA* **2009**, *106*, 15332-15337; (b) C. Y. Jao, A. Salic, *Proc. Natl. Acad. Sci. USA* **2008**, *105*, 15779-15784; (c) J. T. Ngo, D. A. Tirrell, *Acc. Chem. Res.* **2011**, *44*, 677-685.

10.1002/anie.201802972

WILEY-VCH

Entry for the Table of Contents

COMMUNICATION

A sugar sorting pathway directed bioorthogonal reaction confers acidity-independent lysosomal staining and discerns lysosomal pH alterations in necrosis over apoptosis.

Zhongwei Xue, Enkang, Jian Li, Jiahuai Han, and Shoufa Han

Page No. – Page No.

A sugar sorting pathway directed bioorthogonal conjugation enables continual tracking of stressed lysosomes